# Chapter 8
# LEAP-ASIA-2019 Centrifuge Tests at University Gustave Eiffel

**Sandra Escoffier, Zheng Li, and Philippe Audrain**

**Abstract** In the framework of the LEAP-ASIA-2019 exercise, two dynamic centrifuge tests on a gentle slope of saturated Ottawa F-65 sand have been performed at the centrifuge of University Gustave Eiffel. These tests were conducted in parallel with other tests performed in nine other centrifuge centers. In addition to the objectives of the LEAP-UCD-2017 (comparison of the experimental results, e.g., effect of the experimental procedure or of test parameters on the results, and providing of a database for numerical modeling), the new objective was to evaluate, through the tested configuration, the generalized scaling approach described by Iai et al. (Géotechnique 55(5):355–362, 2005). In this framework, all the centrifuge teams have performed two types of tests. Considering the same prototype geometry, the first test was performed following the classical approach used in centrifuge modeling, and the second test was performed considering the generalized scaling law (GSL). Following the test matrix and test specifications of LEAP-ASIA-2019, University Gustave Eiffel has performed two model tests (test A2 renamed UGE-1/50-62 and test A3 renamed UGE-2/25-62). The two tests have been performed on a slope sand with the same relative density (62%) considering a target motion $PGA_{eff}$ = 0.3 g (1 Hz ramped sine at the prototype scale).

In this paper, the test setup and the deviations from the specifications such as the experimental setup improvement that have followed the LEAP-UCD-2017 tests are presented in detail. The results obtained from the two tests are then provided at the prototype scale for comparison. The obtained input base motions are first presented followed by the characterization of the soil through CPT profiles. The responses of the saturated sand slopes for both tests are then detailed through the analysis of the pore pressure buildup, the accelerations in the soil, and the displacements measured through surface markers and embedded sensors. Some preliminary results of the global scaling approach are then discussed.

**Keywords** Liquefaction Experiments and Analysis Projects (LEAP-ASIA-2019) · Generalized scaling law (GSL) · Centrifuge modeling

S. Escoffier (✉) · Z. Li · P. Audrain
Centrifuges for Geotechnics Lab., Univ. Gustave Eiffel, GERS-CG, Bouguenais, France
e-mail: sandra.escoffier@univ-eiffel.fr



T. Tobita et al. (eds.), *Model Tests and Numerical Simulations of Liquefaction and Lateral Spreading II*, https://doi.org/10.1007/978-3-031-48821-4_8

## 8.1 Introduction

Actual researches in numerical modeling on liquefaction phenomena such as advanced numerical technics based on multiscale approach in large deformation (Callari et al., 2010) highlight the need of experimental database for the calibration and the validation processes. In an effort to improve the quality and reliability of the experimental data, a first series of cross tests was performed in the framework of the LEAP-GWU-2015. The analysis of the results, presented in Kutter et al. (2018), highlights that the control of the initial conditions and of the ground motion are key points for cross testing.

Following this first step, one of the objectives of the LEAP-UCD-2017 research program was to provide high-quality laboratory and centrifuge test data. A total of nine centrifuge teams were involved in this experimental research work. Following the model specification document, each team has performed a series of dynamic tests on a gentle slope of saturated Ottawa F-65 sand. The objective of the specifications was to minimize the discrepancies between the experimental procedures followed in each centrifuge team in order to evaluate the quality of liquefaction centrifuge tests and the effects of procedure deviations on the obtained results through cross testing. In addition to this repeatability step, additional tests with different densities and base shaking amplitudes were performed. The objective was to highlight the sensitivity of the response to the soil density and base shaking level. Analysis of the results enabled to conclude that the use of standardized centrifuge CPT is more reliable for soil characterization than the density obtained from weight and dimension measurements (Kutter et al., 2018).

For the next step of the LEAP program, LEAP-ASIA-2019, the new results will be included in the previous database, and they will be compared to the tendencies observed from the previous stages. In addition, the new objective of this LEAP exercise is to provide data to analyze the effectiveness of the generalized scaling law (GSL), described by Iai et al. (2005), for the tested configuration (i.e., gentle submerged slope of sand subjected to a ramped sine loading). In this framework, each of the ten centrifuge teams has performed centrifuge tests at two different centrifuge levels. The first test was performed considering the classical approach used in centrifuge modeling with a scaling factor for centrifuge test of $\eta_1$, and the second test was performed considering the generalized scaling law approach with a scaling factor for $1g$ test of $\mu_2$ and a scaling factor for centrifuge test of $\eta_2$. For both tests, the prototype was the same and the scaling factors were verified $\eta_1 = \eta_2 \times \mu_2$.

In the following, the name of the tests performed highlights the test conditions. The UGE-1/50-62 test refers to a test performed at $50g$ considering a virtual test with a scaling factor of 1, and the UGE-2/25-62 test refers to a test performed at $25g$ considering a virtual test with a scaling factor of 2. In both cases, 62 refers to the relative density (61.6%).

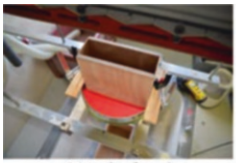

(a) tank of sand

(b) automatic back and forth device

(c) 3 density boxes

**Fig. 8.1** Pluviation setup and density boxes

## 8.2 Test Specifications and Generalized Scaling Laws

### *8.2.1 Target Density*

Following the LEAP-UCD-2017, it was asked to University Gustave Eiffel to perform centrifuge tests on medium dense Ottawa F-65 sand with a target density of 1654 kg.m$^{-3}$. Consequently, a new calibration of the pluviation system has been made. The same pluviation setup was used as in the previous LEAP exercise (Fig. 8.1). Due to the French standard, the selected sieve had an opening of 1.25 mm. This sieve was attached to an automatic hopper that enables back and forth horizontal movements along the whole length of the container (in the *X*-direction), and a sand tank placed above the sieve enables to maintain a constant flow during the pluviation process. To obtain the request density, two slots with an opening width of 25 mm and an axe-to-axe distance of 50 mm were selected. The falling height was fixed at 500 mm, and the length of the opening was sufficient to cover the whole width of the container (in the *Y*-direction) avoiding problems of overlapping for the pluviation process. A density of 1644 kg.m$^{-3}$ was obtained (the average value obtained during the calibration process from three measurements of box density, Fig. 8.1c). Considering the average values of the maximum (1757 kg.m$^{-3}$) and minimum (1490 kg/m$^3$) densities recently provided by Carey et al. (2020), it corresponds to a relative density of 61.6%.

### *8.2.2 Generalyzed Scaling Laws*

Due to the capacity in frequency and acceleration of University Gustave Eiffel shaker, it was asked to perform a first test at 50*g* centrifuge and a second test at 25*g* centrifuge, considering, respectively, a scaling factor for the virtual 1*g* model of 1 and 2. Due to the generalyzed scaling laws, these two configurations should enable to obtain the response of the same prototype. Table 8.1 summarizes the generalized scaling factors for the tests performed at University Gustave Eiffel.

**Table 8.1** Generalyzed scaling factors for the two tests performed at University Gustave Eiffel centrifuge

| | Scaling factors for 1$g$ test | Scaling factors for centrifuge test | Generalized scaling factors | | |
|---|---|---|---|---|---|
| | | | Theoretical expression | UGE-1/50-62 scaling factor ($\mu = 1, \eta = 50$) | UGE-2/25-62 scaling factor ($\mu = 2, \eta = 25$) |
| Length | $\mu$ | $\eta$ | $\mu\eta$ | 50 | 50 |
| Density | 1 | 1 | 1 | 1 | 1 |
| Time | $\mu^{0.75}$ | $\eta$ | $\mu^{0.75}\eta$ | 50 | 42 |
| Frequency | $\mu^{0.75}$ | $1/\eta$ | $\mu^{0.75}/\eta$ | 0.02 | 0.024 |
| Acceleration | 1 | $1/\eta$ | $1/\eta$ | 0.02 | 0.02 |
| Velocity | $\mu^{0.75}$ | 1 | $\mu^{0.75}$ | 1 | 1.68 |
| Displacement | $\mu^{1.5}$ | $\eta$ | $\mu^{1.5}\eta$ | 50 | 70.7 |
| Stress | $M$ | 1 | $\mu$ | 1 | 2 |
| Strain | $\mu^{0.5}$ | 1 | $\mu^{0.5}$ | 1 | 1.4 |
| Stiffness | $\mu^{0.5}$ | 1 | $\mu^{0.5}$ | 1 | 1.4 |
| Permeability | $\mu^{0.75}$ | $\eta$ | $\mu^{0.75}\eta$ | 50 | 42 |
| Pore pressure | $\mu$ | 1 | $M$ | 1 | 2 |

## 8.3 Test Configuration and Procedure

### *8.3.1 Sensor Layout and Container Modifications*

In the case of the tests performed at University Gustave Eiffel, the inner dimensions of the rigid container are 400 mm (L) × 200 mm (W) × 200 mm (H) (Fig. 8.2a). Due to the shaker properties, this container is rigidly fixed with 12 screws inside an ESB container where each corner is blocked with a vertical bar. As for the tests performed in the framework of LEAP-UCD-2017, additional sand was put in place between the outer and inner container to reduce the presence of harmonics due to resonance phenomena of the assembly that were observed during the preliminary tests (Fig. 8.2b).

A cross view and a top view of the sensor layout are presented in Figs. 8.3 and 8.4 in the case of the UGE-1/50-62 test (target coordinates). The target coordinates for the UGE-2/25-62 test are the same.

A total of 10 accelerometers, 6 pore pressure sensors, and 18 surface markers were used. The same markers as for the LEAP-UCD-2017 were used. The diameter of the surface markers was two times smaller than the recommended design (improved design with an external diameter of 13 mm). The locations of the markers in the $X$- and $Y$-directions were performed with a steel rule with a precision of 1 mm, and the $Z$ location was performed with a laser sensor. The precision of the $Z$ position is smaller than 0.5 mm as requested in the specifications. The surface markers have been put in place before the saturation process, and their locations have been measured at 1$g$ before the first spin up of the centrifuge and after each base shaking (Motion #1 and Motion #2) once the centrifuge was spun down.

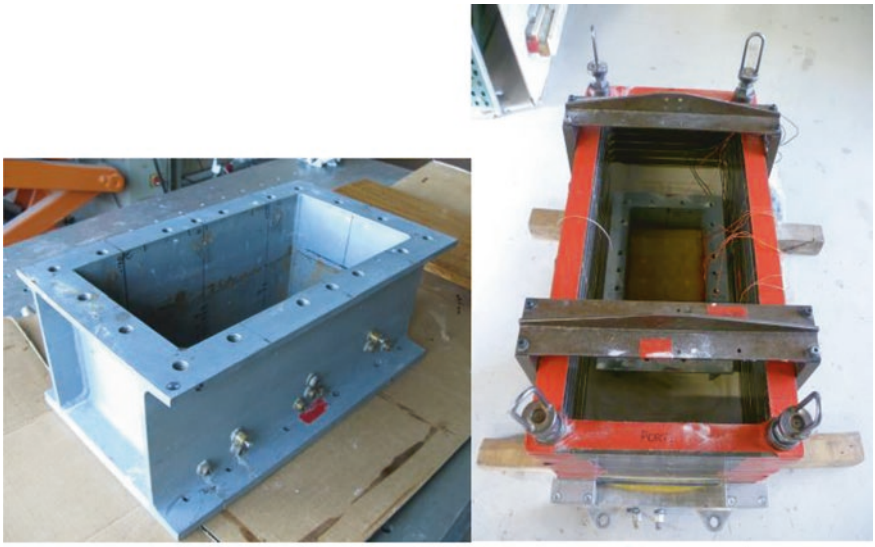


**Fig. 8.2** Rigid steel box especially built for the LEAP project at University Gustave Eiffel and placement of the rigid box inside the blocked ESB container

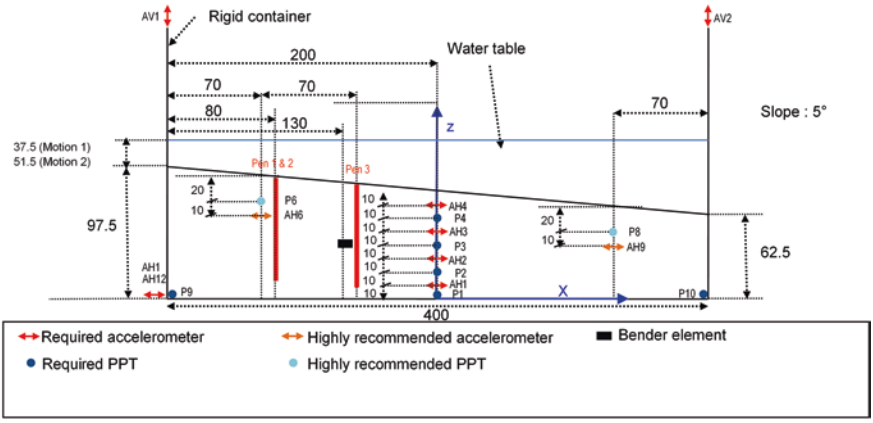


**Fig. 8.3** Cross view of the instrumentation layout of the UGE-1/50-62 test (target coordinates at the model scale in mm)

The shear velocity of the soil was characterized with a pair of bender element that was put in place during the pluviation. The bender elements are of the same type as that described by Brandenberg et al. (2006). Measurements have been made before the first event and after each motion. The analysis of the results is currently underway.

In addition, in both containers, three CPTs were made. In each test, the first, second, and third CPT characterized, respectively, the initial state of the soil and the

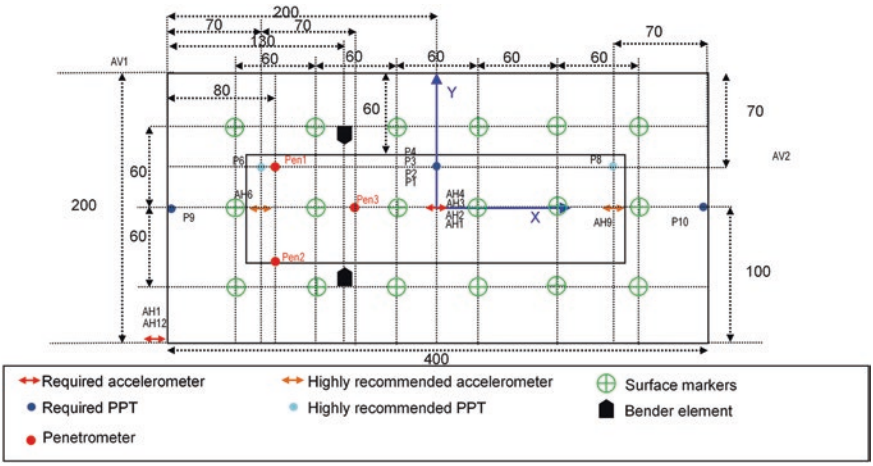


**Fig. 8.4** Top view of the instrumentation layout of the UGE-1/50-62 test (target coordinates at the model scale in mm)

state of the soil after Motion #1 and Motion #2. The CPT used was the one developed at UC Davis (Carey et al., 2018), which has an external diameter of 6 mm. Previously to the centrifuge tests, the CPT was calibrated. The calibration curve highlights a hysteresis (Fig. 8.5) and a new calibration will be done. However, all the data presented for the CPTs take into consideration this initial calibration.

In the case of University Gustave Eiffel 1D shaker, the direction of the solicitation is parallel to the axis of the centrifuge (Chazelas et al., 2008). From the specifications, the radius between the surface of the soil in a transvers cross section and the center of rotation of the centrifuge should be constant. Consequently, the surface should have a circular shape in the direction perpendicular to the base shaking. However, the distance between the axis of rotation of the centrifuge and the center of the soil surface is 5.063 m. Considering that the inner dimension of the container's width is 0.2 m, the difference in height between the midpoint and the corresponding point at the lateral sides should be 1 mm. As this value is in the range of precision of the leveling of the surface, the soil surface was not curved in the *Y*-direction.

### *8.3.2 Viscous Fluid*

In order to verify the scaling law and avoid scaling conflict between the velocity of deformation and the diffusion phenomena, viscous fluid has been used. This viscous fluid is a mixture of tap water, HPMC (Culminal MHPC 50), and biocide that is added in order to avoid the decrease of the viscosity with time (©Kathon biocide).

For the first test, the viscous fluid was obtained by mixing 28 g/l of HPMC powder with 120 ml of biocide (2% of concentration) and 880 ml of tap water based on

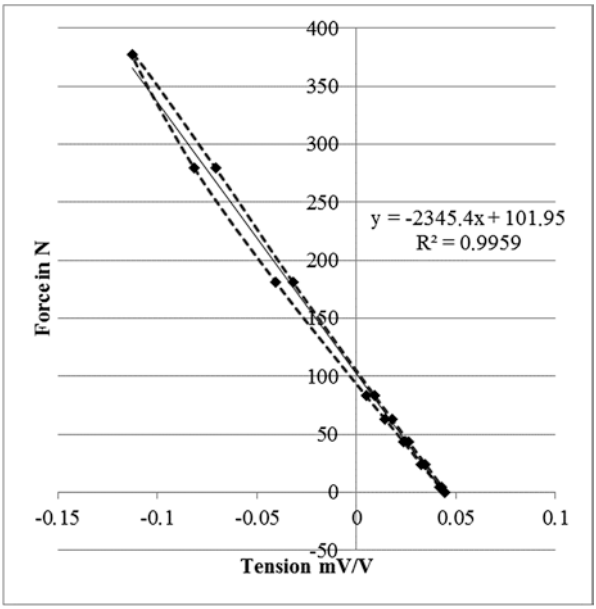


**Fig. 8.5** Calibration of the UC Davis CPT

a series of viscosity measurements and the temperature of the centrifuge room. After 5 days, the viscosity was measured between 64 and 60 cSt for a temperature of 19 °C (measurements at other temperature haven't been performed due to a problem with the thermostatic bath). At the beginning of the UGE-1/50-62 test, the temperature of the centrifuge room was about 18.5 °C. However, due to the small dimensions of the container compared with that of the ESB box usually used, it was decided to introduce after Motion #1 a temperature sensor in the soil. This sensor was introduced at one corner of the box located at the top of the slope ($X = -200$ mm, $Y = 100$). Due to the length of the sensitive part of the sensor, the value is representative of a full-thickness temperature evaluation of the soil/fluid mixture. After the stabilization, the temperature was measured at 26.7 °C. Unfortunately, no viscosity test was performed on the fluid at this temperature during the day of the centrifuge test. After the centrifuge test, viscosity measurements were made but on a fluid taken directly above the soil surface. The viscosity measured was very high between 97 cSt at 19 °C and 73.07 cSt at 26 °C. Among the reasons that can explain such a large difference between the viscosity before and after the test, there is the evaporation. However, the viscosity measurements are sensitive to the presence of impurities. As the fluid was taken above the soil surface, it could have contained impurities. Consequently, these values should be considered with caution.

Therefore, for the second test, UGE-2/25-62, a temperature sensor was introduced at the same location to monitor the temperature before each base shaking. In addition, this measurement, in parallel with viscosity measurement, will be done

during the next step of the LEAP program to increase the relevance of the viscosity value during the base shaking.

### 8.3.3 Saturation Process

Compared to the LEAP-UCD-2017 tests performed by University Gustave Eiffel, the saturation system was improved for the LEAP-ASIA-2019 tests. Figure 8.6 presents the new experimental setup for saturation at 1$g$. The soil container, the viscous fluid tank, and the pump that enables the transfer of the viscous fluid from the tank to the container are all placed in the same vacuum chamber. The lid is a thick plate of Plexiglas that enables to have a top view of all the soil surface during all the saturation process. Once the container, the viscous fluid, and the fluid pump are in place inside the vacuum chamber, a powerful vacuum pump enables to obtain an absolute pressure of 90 mbar in less than 30 minutes. Once this requested absolute pressure is obtained, the vacuum chamber is filled with $CO_2$ up to the atmospheric pressure. Following the saturation process described by Kutter (2013), the absolute pressure is once again decreased up to 90 mbar, and a $CO_2$ flow is once again introduced into the vacuum chamber until the pressure returns to the value of the atmospheric pressure. After a new decrease of the absolute pressure up to 90 mbar, the saturation process starts. As indicated in the LEAP-UCD-2017 specifications, the saturation is made from the surface (at the slope tip), and the fluid pump enables to control the fluid flow all along the process.

At the end of the saturation process, an attempt to evaluate the degree of saturation was made following the method proposed by Okamura and Inoue (2012). However, the measurement did not enable the determination of the degree of saturation due to the sensor noise and, possibly, to the selected target and its fixation.

As previously indicated, the vertical motion of the surface markers was measured using a laser sensor. The use of a laser sensor implies that the source of the laser must be immersed. Due to the minimum distance required between the laser source and the marker, the water level should be at least 35 mm above the top of the

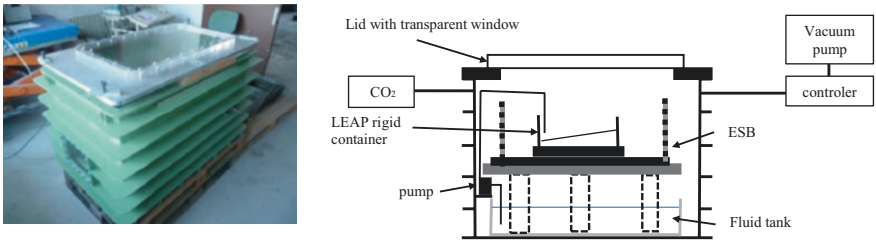


**Fig. 8.6** Saturation setup at 1$g$

slope (Fig. 8.3). At the end of the saturation process, the fluid level was about 1 cm above the top of the slope, and additional viscous fluid was added carefully just before the beginning of the test.

### *8.3.4 Wave Breaker System*

As previously mentioned, due to the use of a laser sensor to record the vertical displacement of the surface markers, a minimum value for the height of the water table above the soil surface was necessary. In the previous LEAP-UCD-2017 exercise (Escoffier & Audrain, 2020), an analysis of the pore water pressure variations measured at the bottom of each extremity of the container (P9 and P10, Fig. 8.2) combined with an analysis of the pore pressure variation measured by the sensors located at 1 m depth near the extremities (P6 and P8, Fig. 8.2) was made. Due to the amplitudes of the pore pressure measured by these four sensors and a phase opposition, it was concluded that one part of the pore pressure fluctuations recorded by these sensors could be due to wave creation. This analysis suggested that a wave reduction system should be built for future tests to avoid non-negligible effect of waves near the extremities of the rigid container.

As a first attempt, a simplified wave breaker was built. Its lower base was in contact with the fluid surface when the container was at rest. The width of the wave breaker was lower than the width of the container. It was assumed that if the wave breaker covers the entire fluid surface, it can create unwanted fluid pressure during the base shaking even if it has not been calculated. Consequently, the width of the wave breaker was 10 cm.

## 8.4 Achieved Ground Motions

### *8.4.1 Horizontal Component*

Figure 8.7 gives the time representation of the achieved motions for the two motions of each test. The data represents the average value obtained from sensors AH11 and AH12. It should be noticed that in the case of the UGE-2/25-62 test, the time at which the maximum value of the 1 Hz component is reached coincides with the time at which the PGA of the raw acceleration is reached. This is not the case for the UGE-1/50-62 test. In this case, the PGA, which is supposed to correspond to the maximum value of the 1 Hz component, has been selected in the time interval $[t_0 + 0.1\ \text{s}, t_0 + 0.1\ \text{s}]$, where $t_0$ is the time at which the maximum value of the 1 Hz component is reached. Considering the effective peak ground accelerations, the values measured in the UGE-2/25-62 are 16–25% higher than that determined in the

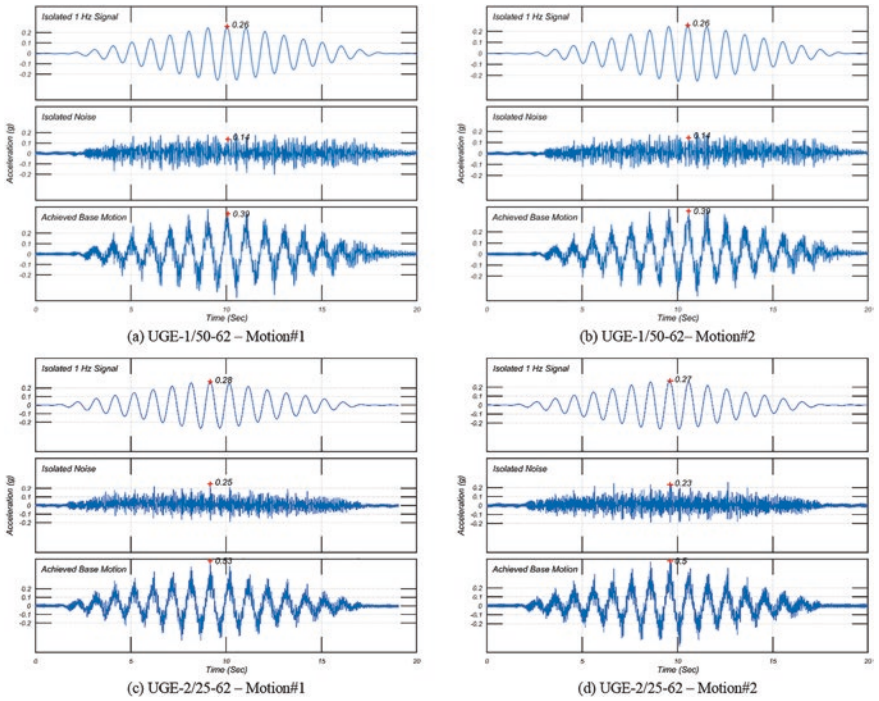


**Fig. 8.7** Achieved base motions for the two tests performed at University Gustave Eiffel (prototype scale)

case of the UGE-1/50-62 test. This difference is essentially due to the level of the noise recorded during the UGE-2/25-62 that is 64–79% higher than that recorded in the UGE-1/50-62 (Table 8.2). Figure 8.8 illustrates the frequency content of the base shaking (average value of the sensors AH11 and AH12). The first five most important frequency components are illustrated by red dots, and the corresponding frequencies are indicated. At the prototype scale, the frequencies of the harmonics are somewhat different between both tests. However, if the values at the model scale for the two first harmonics are considered, they are almost the same for both tests: 380 and 449 Hz for the UGE-1/50-62 test against, respectively, 373 and 458 Hz for the UGE-2/25-62 test. One hypothesis can be that these frequencies correspond to resonance frequencies of the system assembly that are excited in both tests, and due to the generalized scaling law, it induces different frequencies at the prototype scale. However, this hypothesis should be confirmed in the future.

If the characterization of the base shaking is based on Arias intensity, the difference between both tests is less important than if the effective PGA is considered. In the case of Motion #1 and Motion #2, the Arias intensities calculated for the UGE-2/25-62 test are, respectively, 13.6 and 8.8% higher than that calculated for the UGE-1/50-62 test.

**Table 8.2** Characteristics of the achieved base motions (prototype scale)

| Test | Event | $PGA_{eff}$ (g) | 1 Hz component (g) | Other components (g) | Three first main noise frequencies (Hz) | $I_a$ (m/s) |
|---|---|---|---|---|---|---|
| UGE-1/50-62 | Motion #1 | 0.33 | 0.26 | 0.14 | 7.59/8.98/9.63 | 3.95 |
| | Motion #2 | 0.33 | 0.26 | 0.14 | 7.6/8.99/9.67 | 4.19 |
| UGE-2/25-62 | Motion #1 | 0.41 | 0.28 | 0.25 | 8.95/11/14.99 | 4.49 |
| | Motion #2 | 0.385 | 0.27 | 0.23 | 8.97/10.97/14.98 | 4.56 |

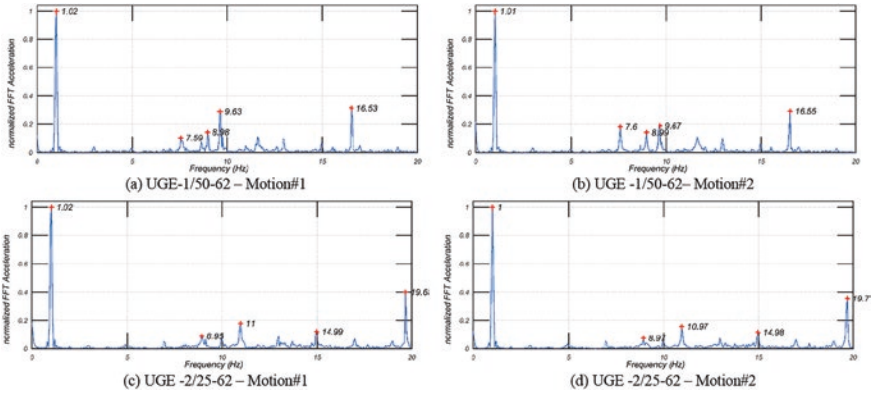


**Fig. 8.8** Frequency content of the achieved base motions for the two tests performed at University Gustave Eiffel (prototype scale)

## *8.4.2 Vertical Component*

The time representation of the vertical components measured at the top of each extremity of the container (AV1 and AV2, Fig. 8.3) is given in Fig. 8.9. Following the analysis of the vertical components made by Kutter et al. (2018), a pass band filter [0.3–3 Hz] has been applied to the raw data for analysis. A FIR filter (finite impulse response filter windowed with a Chebyshev window) was used. Considering all the tests, the maximum vertical filtered acceleration remains lower than 0.015 g. However, the vertical behavior is not constant. In the UGE-1/50-62 test for Motion #2, there is a phase opposition that indicates a rotation of the container. In the same test for Motion #1, the vertical accelerations are not the same at both extremities, but they are in phase. For the second test, UGE-2/25-62, the vertical accelerations are somewhat the same and in phase for Motion #1, whereas they are different and present a phase difference for Motion #2.

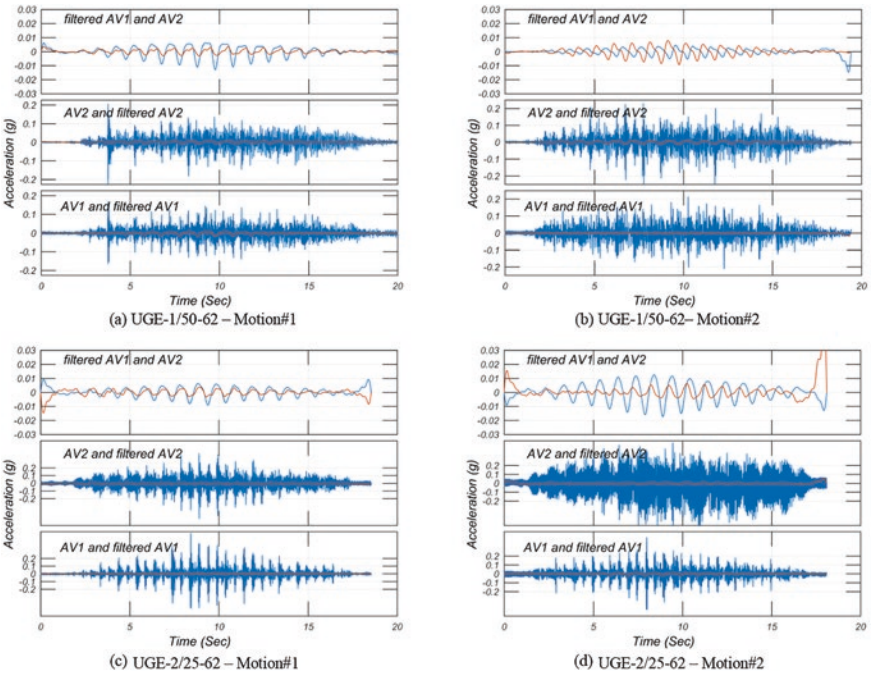


**Fig. 8.9** Time representation of the vertical raw and filtered accelerations at both extremities of the rigid container (prototype scale)

## 8.5 Results

In this part, all the data are presented at the prototype scale using the generalized scaling laws presented in Table 8.1.

### *8.5.1 CPT Results*

The CPT profiles are presented in Fig. 8.10 for each test. In the case of the UGE-2/25-62 test, the depth of investigation was lower than for the other test, and the recorded data were noisy. No noticeable evolution is recorded between the CPTs performed at the initial state and after both motions in the case of the UGE-2/25-62 test (Fig. 8.10b). The $q_c(z)$ profile is almost the same as the $q_c(z)$ profile that was obtained for the initial state of the soil column in the UGE-1/50-62 test. For this last test, successive base shakings induced a modification of the $q_c$ profile: the profile increases with successive shaking indicating a densification of the soil. This result is in accordance with the liquefaction phenomena. It can be noticed that the peak

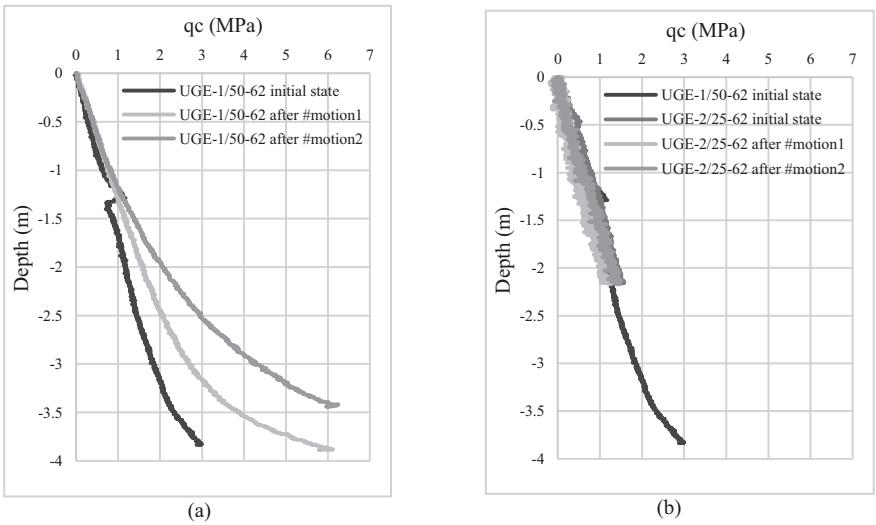


**Fig. 8.10** CPT results for both University Gustave Eiffel test at the prototype scale (**a**) UGE-1/50-62 test and (**b**) UGE-2:25-62 test and initial CPT profile of UGE61/50-62

that appeared in the case of the $q_c$ profile for the initial state of the UGE-1/50-62 test is supposed to be due to the presence of a cable of a pore pressure sensor.

### *8.5.2 Pore Pressure Response*

Figure 8.11 shows the pore water pressure response of the central array of pore pressure sensors. Considering the positioning of the sensors during the pluviation process, the initial vertical effective stresses for the P1 and P3 sensors in the case of the UGE-1/50-62 test were, respectively, 38.9 and 18.2 kPa. In the case of the UGE-2/25-62 test, the initial vertical effective stresses for P1 to P4 were, respectively, 38.9, 30.3, 23.7, and 9.1 kPa. These limits are indicated in black dotted horizontal lines in Fig. 8.11.

During the first base shaking, the evolution of the pore pressure observed for P1 and P3 is comparable in both tests. The pore pressure buildup is a little noisier in the case of the UGE-2/25-62 test. The pore pressure buildup reached the initial effective stress at 2 m depth. At 4 m depth, the pore pressure buildup is somewhat lower than the initial vertical effective stress, and the value of $r_u = 1$ is only reached on a very limited time (this value is only reached for few pore pressure peaks in the case of UGE-2/25-62, and the maximum value of $r_u$ reached for UGE-1/50-62 is 0.96).

In the case of UGE-2/25-62, the pore pressure buildup recorded at 3 and 1 m depth indicates liquefaction ($r_u = 1$) for both levels.

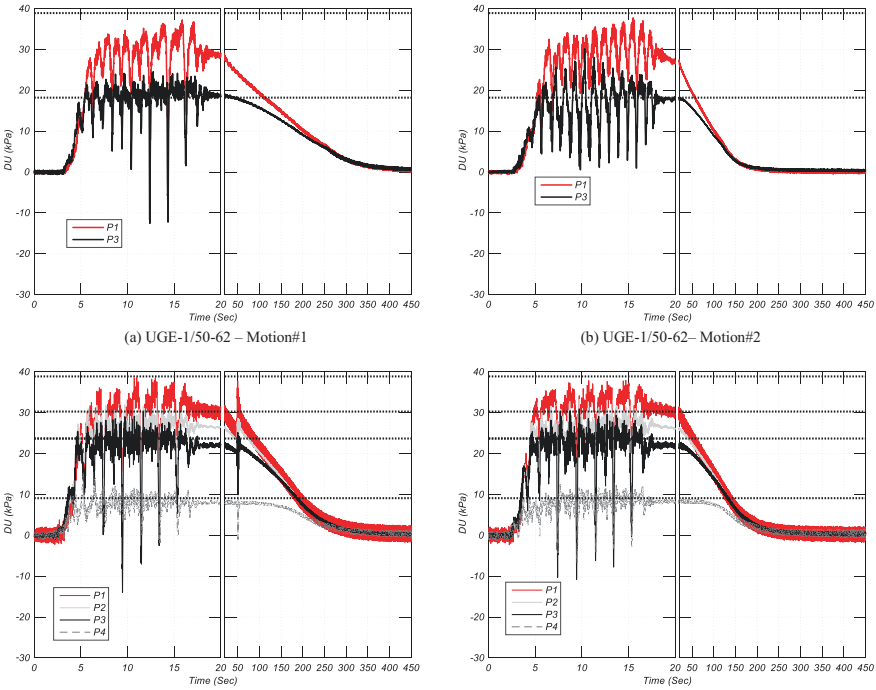


(a) UGE-1/50-62 – Motion#1

(b) UGE-1/50-62– Motion#2

(c) UGE-2/25-62 – Motion#1

(d) UGE-2/25-62 – Motion#2

**Fig. 8.11** Pore pressure buildup during and after the base shaking

In addition, for both tests, some spikes appear during Motion #1, more specifically at 2 and 3 m depth, indicating a deliquefaction phenomenon (cyclic mobility-dilatancy phenomena).

In the case of Motion #2, the time histories of the pore pressure buildup were somewhat different between the two tests. No noticeable evolution appeared between the first and the second motion applied on UGE-2/25-62. On the contrary, the pore pressure buildup for the second motion applied on UGE-1/50-62 presents greater cyclic variation of pore pressure with less noticeable pore pressure spikes.

Concerning the pore pressure decay after the base shaking, it is somewhat difficult to compare both tests in the case of the first motion; as for the UGE-2/25-62 test, an aftershock took place and induced new pore pressure buildup. However, in the case of Motion #2, the pore pressure decays are somewhat the same in both tests. As previously mentioned, in the case of the UGE-1/50-62, the value of 73.07 cSt measured after the test on a sample of fluid drawn in the fluid layer above the soil surface should be considered with caution. The obtained results on the pore pressure decay after the second motion tend to confirm that this measured viscosity is not reliable.

As mentioned for the previous tests performed in the framework of the LEAP-UCD-2017, regarding the amplitude and the phase of the pore pressure measured by pore pressure sensors P10, P9, P8, and P6 (Fig. 8.2) and their initial depth, it was supposed that one part of the pore pressure fluctuations recorded by these four sensors was due to the waves created during the base shaking. These previous results

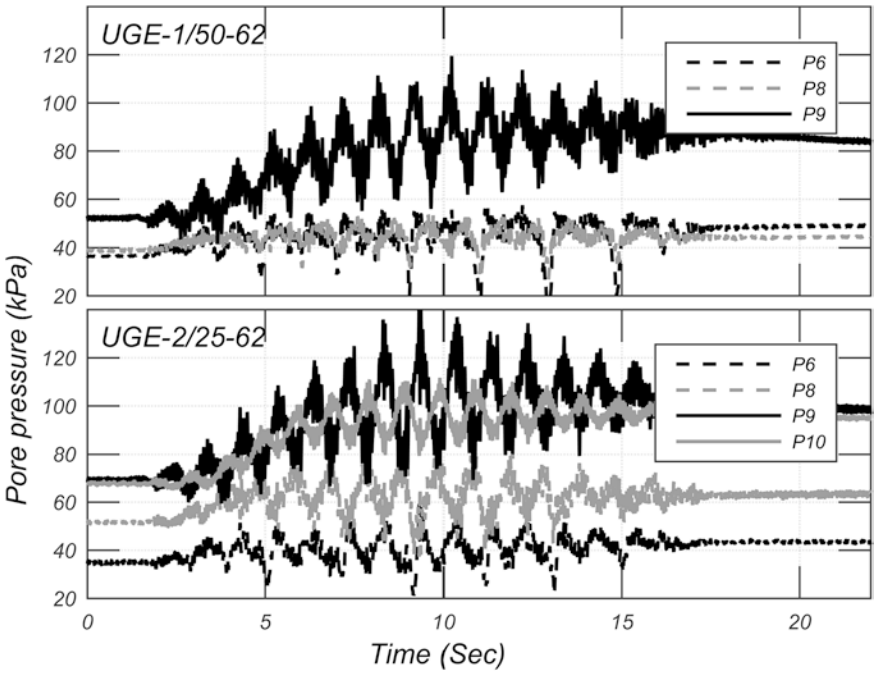


**Fig. 8.12** Motion #1 pore pressure buildup during and after the base shaking – wave breaker effect

suggested the use of a wave breaker system to avoid non-negligible effects of waves near the extremities of a rigid container (the pore pressure measurement located in the center of the container was less influenced by the waves). Consequently, a wave breaker was built for the LEAP-ASIA-2019 exercise. Figure 8.12 illustrates the pore pressure evolution measured by the sensors P10, P9, P8, and P6 during Motion #1 of the UGE-1/50-62 and UGE-1/25-62 tests. For the first test, the wave breaker was not in place contrary to the second test. Without wave breaker, the three pore pressure measurements P9, P8, and P6 (P10 was out of order) are in phase. The maximum theoretical values of pore pressure calculated from the sensor locations and the viscous fluid level at rest were compared to the maximum value reached during the test. The maximum measured values reached by P9, P8, and P6 were 119, 62, and 68 kPa against 116, 50, and 49 kPa from the theoretical values. In the case of the test UGE-2/25-62, during the which one a wave breaker was used, the sensors P9 and P10, and P6 and P8, were respectively in phase opposition. The maximum pore pressure values recorded by sensors P10, P9, P8, and P6 were, respectively, 112, 143, 87, and 59 kPa. As for the test without wave breaker, they were larger than the theoretical one (respectively, 100, 111, 65, and 50 kPa).

The comparison of these two results highlights a difference in behavior between the two tests: if the measured pore pressures remain higher than the theoretical ones in both tests, the phase difference between the pore pressure measurements is not the same. Results from the UGE-2/25-62 test seem to indicate the presence of wave, and, on the contrary, there is no clear evidence of waves in the UGE-1/50-62 test.

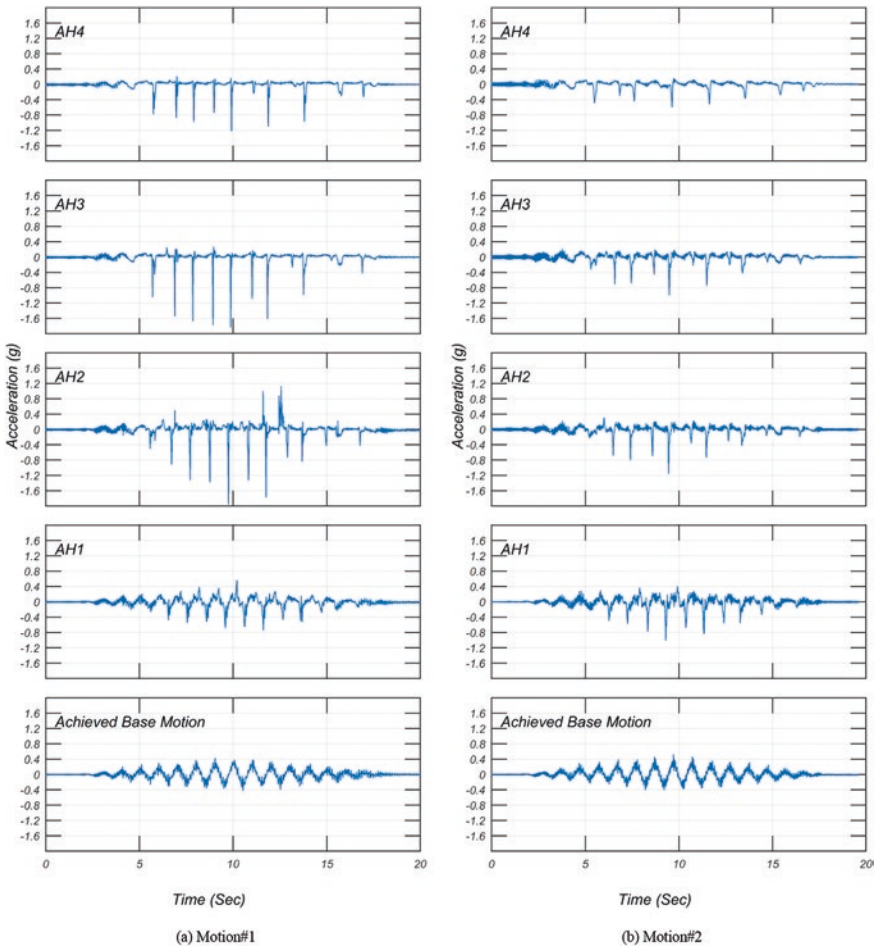


**Fig. 8.13** UGE-1/50-62: time history of the acceleration measured by the central array of accelerometers

This difference can be induced by the differences between the two tests due to the use of the GSL and/or the wave breaker. However, there is a clear evidence that the wave breaker should be improved.

### *8.5.3 Acceleration Response*

The time histories of the accelerations measured by accelerometers AH1 to AH4 are presented in Figs. 8.13 and 8.14 for, respectively, the UGE-1/50-62 and UGE-2/25-62 tests. The global behavior observed in both tests is comparable.

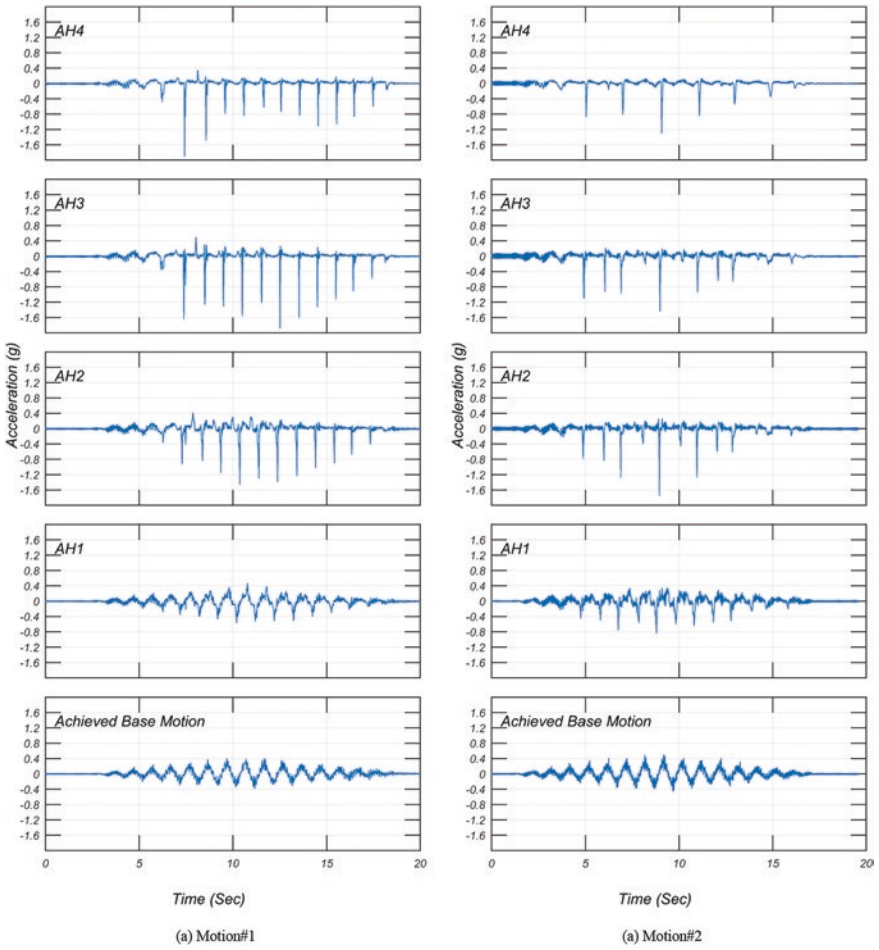


**Fig. 8.14** UGE-2/25-62: time history of the acceleration measured by the central array of accelerometers

At the beginning of Motion #1, the time acceleration at 3.5 m depth (AH1) still followed the trace of the base input motion. However, after four cyclic loadings, small spikes started to appear, and even if cyclic variations of acceleration were still noticeable, they deviated from the base shaking. At 2.5 m depth (AH2) and above (AH3 and AH4), the initiation of liquefaction was observed. It is characterized by sharp spikes of acceleration that are evidence of shock waves induced by deliquefaction phenomena (Kutter & Wilson, 1999). Considering the beginning of the loading, the liquefaction occurred first near the surface, and then the phenomenon was spreading in depth. However, there was small phase lag between 0.5 and 2.5 m depth.

As previously mentioned, except in the case of the second motion in the UGE-50/1-62 test, where time history of the pore pressure presented greater cyclic

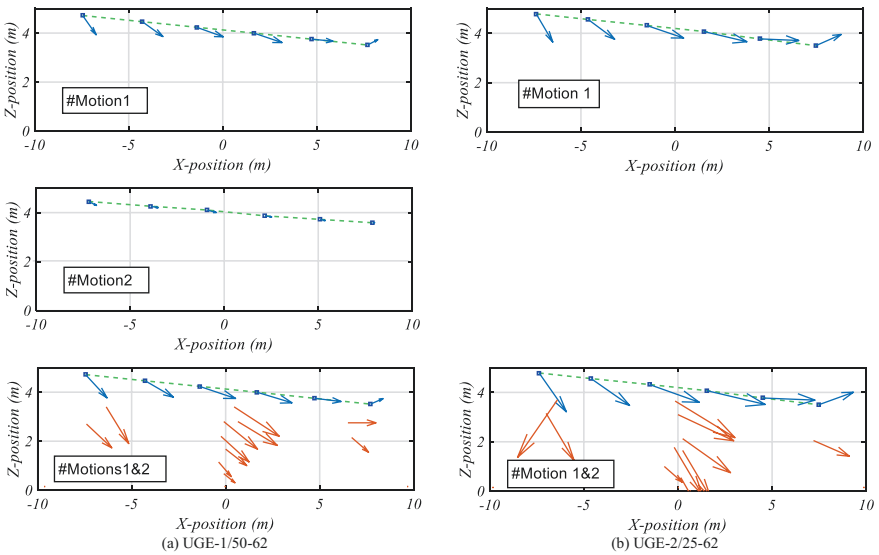


**Fig. 8.15** Surface markers (blue arrows) and embedded sensor displacement (red arrows) induced by Motion #1, Motion #2, and Motions #1 and #2, for both centrifuge tests performed at University Gustave Eiffel

variation with less noticeable pore pressure spikes, the time histories of the pore pressure buildup in the other cases were similar.

There was no noticeable effect of Motion #1 on the time histories of the pore pressure observed during Motion #2. The observed time histories of the acceleration are in accordance with these results: in the case of Motion #2, the UGE-1/50-62 test presents smaller acceleration spikes than for the other cases.

### *8.5.4 Surface Marker Responses*

Cross views of the residual displacements of the surface markers induced by Motion #1 and Motion #2 are presented in Fig. 8.15. For Motion #1, the initial positions of the surface markers correspond to the first position measurements before the first spin up of the centrifuge. For Motion #2, only the results for the direct approach are provided, and the initial positions were obtained considering the residual displacement induced by Motion #1. In order to enhance the displacements and compare the results of both tests, the length of the displacement vectors was magnified by 3.

In the case of the surface displacements induced by Motion #1, the directions of the displacements are somewhat the same in both tests (Table 8.3). However, larger displacements are observed when GSL are concerned (UGE-2/25-62). If the average values of the displacement obtained from the surface markers with the same $X$ location are considered, the residual displacements observed when GSL is

**Table 8.3** Average[a] displacement amplitude and orientation calculated from the measured displacements of the surface markers – Motion #1

| Motion #1 | Amplitude (m) | | | Orientation (°) | | |
|---|---|---|---|---|---|---|
| Marker number | UGE-1/50-62[a] | UGE-2/25-62[a] | Relative difference in %[b] | UGE-1/50-62[a] | UGE-2/25-62[a] | Relative difference[b] |
| 1 | 0.358 | 0.483 | 35 | −47.5 | −52.4 | 10 |
| 2 | 0.419 | 0.542 | 29 | −28.9 | −29.6 | 2 |
| 3 | 0.493 | 0.682 | 38 | −15.4 | −14.5 | −6 |
| 4 | 0.517 | 0.778 | 50 | −14.6 | −10.23 | −30 |
| 5 | 0.384 | 0.696 | 81 | −4.1 | −1.8 | −56 |
| 6 | 0.198 | 0.473 | 139 | 22 | 18.7 | −15 |

[a]The values correspond to the average value of the displacement amplitude and inclination calculated from the three markers located at the same X position. The inclination is relative to the horizontal plane

[b]The relative difference is calculated considering the UGE-1/50-62 test as a reference

concerned are 29–139% higher than that obtained in the UGE-1/50-62 test (Table 8.3).

In order to highlight the effect of the previous base shaking on the surface displacement, the displacements associated with the second base shaking are represented in the case of the UGE-1/50-62 test. The observed displacements are largely lower than that induced by the first event. This decrease can be due to the densification of the soil induced by the liquefaction that took place during Motion #1. This analysis is more complex in the case of the UGE-2/25-62 test due to scaling conflict between the displacement and the length. Consequently, only the total displacement induced by the combined effect of both motions is represented for both tests. In this case, the total displacements of the embedded sensors are also represented by red arrows in Fig. 8.15. The difference between the displacement amplitudes and their orientations between the two tests are comparable to that observed for the first motion (Table 8.4). In the case of UGE-2/25-62, based on GSL, the displacements were 38–168% higher than in the other test with larger difference at the bottom of the slope. The difference in the direction varies between 6% and −67% indicating that, at the top of the slope, the residual displacement of the soil is more downward and, near the bottom of the slope, more upward when GSL is considered (UGE-2/25-62).

## 8.6 Conclusions

This paper summarized the experimental setup, the followed experimental procedure, and some results of the two centrifuge tests performed at University Gustave Eiffel in the framework of the LEAP-ASIA-2019 series of tests.

Two centrifuge tests were performed by University Gustave Eiffel. The tests were done on a medium dense Ottawa F-65 sand. The first test was performed at 50*g*

**Table 8.4** Average displacement amplitude and orientation calculated from the measured displacements of the surface marker cumulative effect of Motions #1 and #2

| Motions #1 and #2 | Amplitude (m) | | | Orientation (°) | | |
|---|---|---|---|---|---|---|
| Marker number | UGE-1/50-62 | UGE-2/25-62 | Relative difference in %* | UGE-1/50-62 | UGE-2/25-62 | Relative difference* |
| 1 | 0.498 | 0.714 | 43 | −39.7 | −47.4 | 19 |
| 2 | 0.547 | 0.774 | 41 | −24 | −28.0 | 17 |
| 3 | 0.662 | 0.916 | 38 | −14.4 | −15.2 | 6 |
| 4 | 0.642 | 1.054 | 64 | −13.0 | −10.2 | −22 |
| 5 | 0.477 | 0.932 | 95 | −5.4 | −1.8 | −67 |
| 6 | 0.237 | 0.636 | 168 | 18.6 | 15.4 | −17 |

centrifuge and the second test at 25*g*. Considering the GSL approach, tests were scaled to represent the same prototype.

The main deviation from the specifications was the viscosity of the fluid for the UGE-1/50-62 test for which the viscosity is assumed higher than the requested one, despite no precise determination is available. However, based on the comparison of the pore pressure dissipation after the second base shaking in both tests, doubts might be raised on the validity of viscosity measurements that has been performed after the test.

Compared to the previous tests performed in the framework of LEAP-UCD-2017 exercise, an improved system of saturation was used, which enabled a better control of the fluid flow and less leakage due to its configuration.

The 1 Hz horizontal component of the base shaking at the base of the container was similar between the tests. The noise was somewhat higher in the case of the UGE-2/25-62 test inducing a $PGA_{eff}$ 15–25% higher than for the UGE-1/50-62 test. This difference decreases to 13.6% up to 8.8% if the Arias intensity is considered.

The vertical motions at the top of the container weren't the same between the different motions and between the tests. Difference between the tests can be due to the difference of frequency for the base shaking that can induce different response of the experimental assembly. However, the difference of response between the motions of the same test is not actually explained.

Considering the results obtained, the characterization of the soil column through CPT measurement highlights a difference between the two tests: in the case of the GSL, no noticeable evolution of the CPT profile was recorded, while the CPT profile increases with the successive motion for the test that is not based on GSL. However, the noisy response obtained for the second test can be relevant of the problem with the experimental setup in this case. For the next LEAP exercise, a new calibration of the CPT will be made, and more caution will be taken for the CPTs.

The global scaling approach seems to give good results if the acceleration and the pore pressure buildup are considered. However, due to a problem with the fluid viscosity, these tests cannot be considered as relevant for the analysis of the global scaling approach when it concerns the pore pressure dissipation after the base shaking.

On the contrary, when the displacements are considered, large discrepancies appear especially in terms of amplitude and, to a lesser extent, in terms of orientation of the displacement.

**Acknowledgments** This experiment has been made in the framework of the LEAP-ASIA-2019 series of experiments. The authors would like to thank all the participating centrifuge teams that share their knowledge.

## References

Brandenberg, S. J., Choi, S., Kutter, B. L., Wilson, D. W., & Santamarina, J. C. (2006). A bender element system for measuring shear wave velocities in centrifuge models. *Proceedings, 6th international conference on physical modeling in geotechnics*, p 165–170. https://nees.org/data/get/NEES-2006-0149/Documentation/References/Brandenberg_2006.pdf

Callari, C., Armero, F., & Abati, A. (2010). Strong discontinuities in partially saturated poroplastic solids. *Computer Methods in Applied Mechanics and Engineering, 199*, 1513–1535.

Carey, T., Gavras, A., Kutter, B., Haigs, S. K., Madabushi, S. P. G., Okamura, M., Kim, D. S., Ueda, K., Hung, W. Y., Zhou, Y. G., Liu, K., Zeghal, M., Abdoun, T., Escoffier, S., & Manzari, M. (2018). A new shared miniature cone penetrometer for centrifuge testing. In A. MCNamara, S. Divall, R. Goodey, N. Taylor, S. Stallebrass, & J. Panchal (Eds.), *ICPMG 2018* (Vol. 1, pp. 293–298).

Carey, T., Stone, N., & Kutter, B. L. (2020). Grain size analysis and maximum and minimum dry density testing of OTTAWA F-65 Sand for LEAP-UCD-2017. In B. L. Kutter, M. T. Manzari, & M. Zeghal (Eds.), *Model tests and numerical simulation of liquefaction and lateral spreading LEAP-UCD-2017* (pp. 31–44). Springer, ISBN 978-3-030-22817-0.

Chazelas, J.-L., Escoffier, S., Garnier, J., Thorel, L., & Rault, G. (2008). Original technologies for proven performances for the new LCPC earthquake simulator. *Bulletin of Earthquake Engineering, 6*(4), 723–728.

Escoffier, S., & Audrain, P. (2020). LEAP-UCD_2017 centrifuge test at University Gustave Eiffel. LEAP-UCD-2017. *Reproducibility and sensitivity of centrifuge tests and comparisons to simulations of lateral spreading*, to be published, pp. XXX.

Iai, S., Tobita, T., & Nakahara, T. (2005). Generalised scaling relations for dynamic centrifuge tests. *Géotechnique, 55*(5), 355–362.

Kutter, B. L. (2013). Effects of capillary number, bond number, and gas solubility on water saturation of and specimens. *Canadian Geotechnical Journal, 50*(2), 133–144.

Kutter, B. L., & Wilson, D. W. (1999). De-liquefaction shock waves. *Proceedings, 7th US-Japan workshop on earthquake resistant design of lifeline facilities and countermeasures against soil liquefaction, MCEER-99-0019*, pp. 295–310.

Kutter, B. L., Carey, T. J., Hashimoto, T., Zeghal, M., Adboun, T., Kokkali, P., Madabhushi, G., Haigh, S., Burali d'Arezzo, F., Madabhushi, S., Hung, W. Y., Lee, C. J., Chegn, H. C., Iai, S., Tobita, T., Zhou, Y. G., Chen, Y., Sun, Z. B., & Manzari, M. T. (2018). Leap-GWU-2015 experiment specifications, results, and comparisons. *Soil Dynamics and Earthquake Engineering, 113*, 616–628.

Okamura, M., & Inoue, T. (2012). Preparation of fully saturated model for liquefaction study. *International Journal of Physical Modelling in Geotechnics, 12*(1), 39–46.